scientific reports

Check for updates

OPEN

Superconductivity in In-doped $AgSnBiTe_3$ with possible band inversion

Tsubasa Mitobe[1], Kazuhisa Hoshi[1], Md. Riad Kasem[1], Ryosuke Kiyama[1], Hidetomo Usui[2], Aichi Yamashita[1], Ryuji Higashinaka[1], Tatsuma D. Matsuda[1], Yuji Aoki[1], Takayoshi Katase[3], Yosuke Goto[1] & Yoshikazu Mizuguchi[1]✉

We investigated the chemical pressure effects on structural and electronic properties of SnTe-based material using partial substitution of Sn by $Ag_{0.5}Bi_{0.5}$, which results in lattice shrinkage. For $Sn_{1-2x}(AgBi)_xTe$, single-phase polycrystalline samples were obtained with a wide range of x. On the basis of band calculations, we confirmed that the $Sn_{1-2x}(AgBi)_xTe$ system is basically possessing band inversion and topologically preserved electronic states. To explore new superconducting phases related to the topological electronic states, we investigated the In-doping effects on structural and superconducting properties for $x = 0.33$ ($AgSnBiTe_3$). For $(AgSnBi)_{(1-y)/3}In_yTe$, single-phase polycrystalline samples were obtained for $y = 0$–0.5 by high-pressure synthesis. Superconductivity was observed for $y = 0.2$–0.5. For $y = 0.4$, the transition temperature estimated from zero-resistivity state was 2.4 K, and the specific heat investigation confirmed the emergence of bulk superconductivity. Because the presence of band inversion was theoretically predicted, and the parameters obtained from specific heat analyses were comparable to In-doped SnTe, we expect that the $(AgSnBi)_{(1-y)/3}In_yTe$ and other (Ag, In, Sn, Bi)Te phases are candidate systems for studying topological superconductivity.

Metal tellurides (MTe) with a NaCl-type structure have been extensively studied due to their physical properties as topological materials[1–4], thermoelectric materials[5–7], and superconductors[8–12]. Among them, In-doped SnTe superconductors have been drawing attention as a candidate system of a topological superconductor[4,13–17]. SnTe is a topological crystalline insulator, and superconductivity is typically induced by In-doping at the Sn site. The superconducting transition temperature (T_c) of (Sn, In)Te increases by In doping. Although a simple picture proposes that doped In acts as a hole dopant, detailed analyses of carrier characteristics, superconducting properties, and electronic states of (Sn, In)Te revealed that the In doping does not simply act as a dopant of holes, but the superconductivity emerges in a regime where electron carriers are dominant[16]. Therefore, to understand the nature and the mechanisms of superconductivity in SnTe-based, development of new superconductors based on NaCl-type tellurides is important.

In MTe, the M site can be alloyed flexibly. For example, single crystals (films) of (Sn, Pb)Te can by grown with a wide solution range, and the alloy system has provided a platform to study topological nature of MTe[1,18,19]. Because the Pb substitution for SnTe expands the lattice, which corresponds to negative chemical pressure at the M–Te bond, contrasting positive chemical pressure in MTe leads the way for further expanding the research field of superconductivity in MTe. In addition, although In-doped systems of (In, Sn, Pb)Te have been studied as a topological superconductor candidate[20], there has been no detailed study on superconducting properties and crystal structure of NaCl-type MTe with a lattice constant smaller than SnTe. In this study, we focused on the (Ag, Sn, Bi)Te system that has been studied as a thermoelectric material and found that the (Ag, Sn, Bi)Te system is possible topological material[21,22]. In SnTe, Sn is divalent, Sn^{2+}. When $Ag^{+}_{0.5}Bi^{3+}_{0.5}$ substitutes Sn^{2+}, the total valence states (charge neutrality) has been preserved. Therefore, the $Ag_{0.5}Bi_{0.5}$ substitution for the Sn site is successfully achieved in a wide range up to the end member of $AgBiTe_2$. Here, we show the evolution of the structural and electronic characteristics of $Sn_{1-2x}(AgBi)_xTe$. Then, we report superconductivity induced by In substitution in $(AgSnBi)_{(1-y)/3}In_yTe$.

[1]Department of Physics, Tokyo Metropolitan University, 1-1, Minami-osawa, Hachioji 192-0397, Japan. [2]Department of Physics and Materials Science, Shimane University, 1060, Nishikawatsucho, Matsue 690-8504, Japan. [3]Laboratory for Materials and Structures, Institute of Innovative Research, Tokyo Institute of Technology, 4259 Nagatsuta, Midori, Yokohama 226-8503, Japan. ✉email: mizugu@tmu.ac.jp

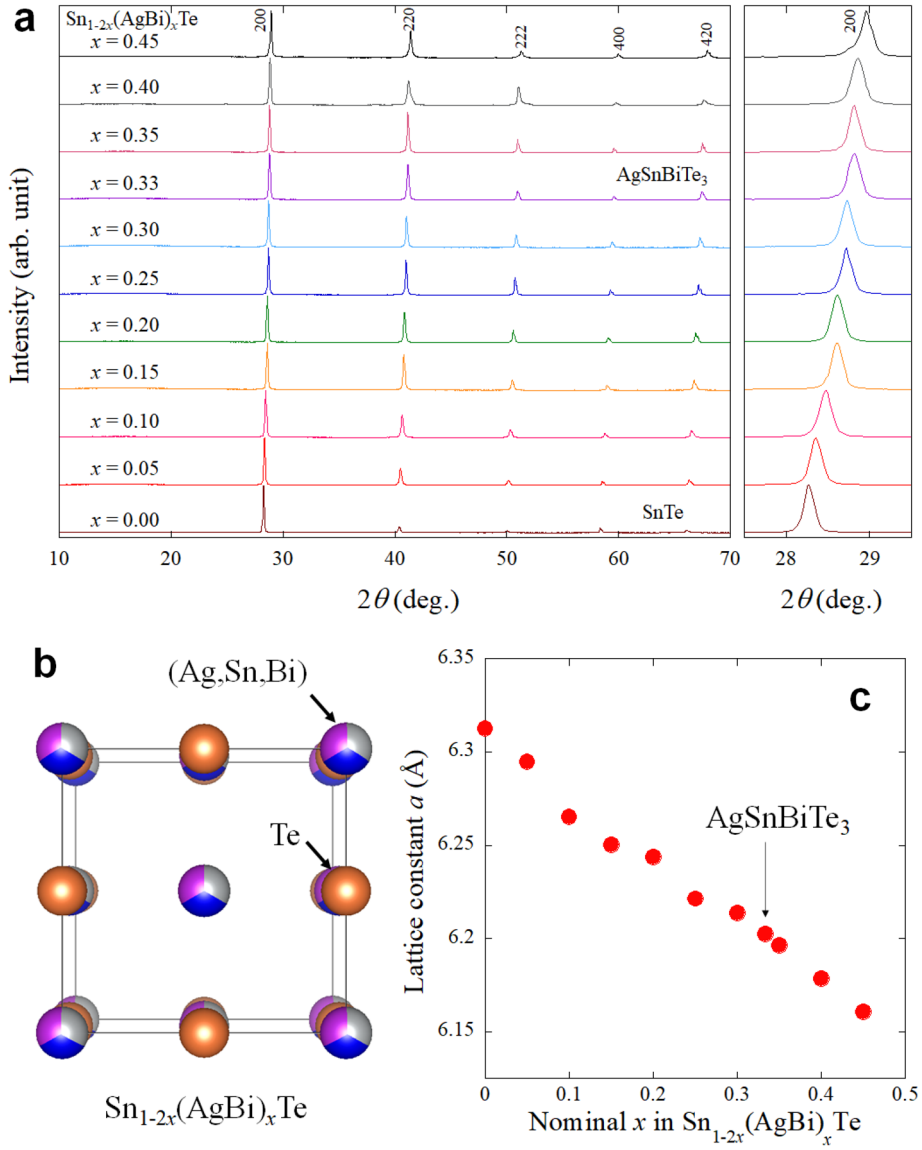

Figure 1. Crystal-structure evaluation of $Sn_{1-2x}(AgBi)_xTe$. (**a**) XRD patterns of $Sn_{1-2x}(AgBi)_xTe$. (**b**) Schematic image of the NaCl-type crystal structure of $Sn_{1-2x}(AgBi)_xTe$. (**c**) x dependence of the lattice constant.

Results and discussion

Structural and electronic characteristics of $Sn_{1-2x}(AgBi)_xTe$. As mentioned above, the (Ag, Sn, Bi) Te system would be an important system to expand the material variety of SnTe-based compounds including new superconductors. We started this work by investigating lattice compression in $Sn_{1-2x}(AgBi)_xTe$, in which x corresponds to the total amount of Ag and Bi substituted for the Sn site in the SnTe structure. Polycrystalline samples of $Sn_{1-2x}(AgBi)_xTe$ were synthesised by a melting method. Figure 1a shows the X-ray diffraction (XRD) patterns for $Sn_{1-2x}(AgBi)_xTe$. The XRD peaks correspond to that expected for the NaCl-type structure (Fig. 1b) and systematically shift to higher angles, which indicates lattice shrinkage with increasing x. The lattice constant a was determined by Rietveld refinements and plotted in Fig. 1c. The trend is consistent with previous reports[20,21]. In the refinements, Ag, Sn, and Bi were assigned to the M site as shown in Fig. 1b, and the nominal composition (fixed) was used. Since we used laboratory XRD in this study, isotropic displacement parameter B_{iso} was fixed to 1 for all sites.

Figure 2 shows the calculated band structure for SnTe with various lattice constants of 6.6, 6.4, 6.3 (close to the lattice constant of SnTe), and 6.1 Å. By calculating the lowest energy of the Sn-p orbital and the highest energy of the Te-p orbital at the L point in reciprocal space, we confirmed that a band inversion transition occurs at around $a = 6.35$ Å (Fig. 2e). Note that the contributions of Sn-p orbitals are represented by the size of the circle symbols in Fig. 2a–d. Furthermore, calculation results with a smaller lattice constant show that SnTe-based materials with a small lattice constant of 6.1 Å also shows a band inversion. The observed trend is consistent with a previous theoretical work on SnTe and PbTe systems[2]. Therefore, we consider that the current system of $Sn_{1-2x}(AgBi)_xTe$ basically possesses a topologically-preserved band structure with a wide range of x. Although calculations in this

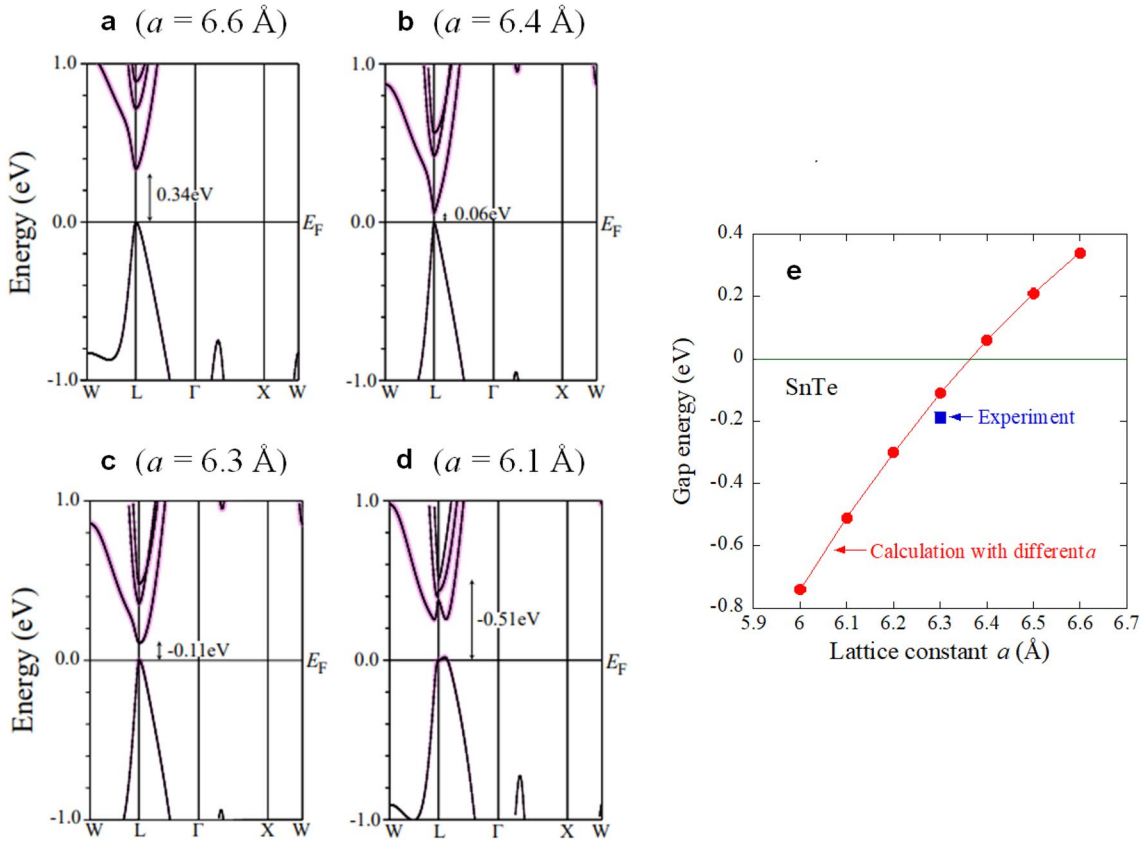

Figure 2. Electronic structure for SnTe with various lattice constants. (**a**–**d**) Calculated band structure. Contribution of Sn-*p* orbitals is represented by the size of pink-circle symbol. According to the calculations, a band inversion occurs with lattice constants smaller than 6.35 Å as plotted in (**e**). Experimental data in Ref.[23] is plotted. Gap energy was calculated from the lowest energy of the Sn-p orbital and the highest energy of the Te-*p* orbital at the L point.

work have been performed on SnTe with different lattice constants, no obvious modification of the band structure is expected when Sn was partially replaced by $Ag_{0.5}Bi_{0.5}$ in real materials because the difference in spin–orbit interactions expected from those elements is not large. Since the orbital characteristics in the band structure does not largely change between SnTe and $Sn_{1-2x}(AgBi)_xTe$, we consider that the topological invariant in this system is mirror Chern number from the analogy to SnTe, which suggests that the $Sn_{1-2x}(AgBi)_xTe$ system is a potential topological crystalline insulator. On the basis of the investigations of lattice constant and band structure for the SnTe-based system $Sn_{1-2x}(AgBi)_xTe$, we selected $AgSnBiTe_3$ ($x = 0.33$) for a parent phase in which In-substitution effects are examined in this study.

Superconducting properties of $(AgSnBi)_{(1-y)/3}In_yTe$. For the In-doped $AgSnBiTe_3$ system (see Fig. 3c for crystal structure), we used a chemical formula, $(AgSnBi)_{(1-y)/3}In_yTe$, because the In amount doped to the parent phase of $AgSnBiTe_3$ can be easily understood. Figure 3a shows the powder XRD patterns of $(AgSnBi)_{(1-y)/3}In_yTe$; the In-doped samples were synthesised by high-pressure annealing. As shown in Fig. 3b, Rietveld refinement reveals that tiny (shoulder) anomaly was observed. Such a shoulder structure would be due to the presence of inhomogeneous regime with a slightly different lattice constant and was observed in NaCl-type tellurides containing multiple *M*-site elements[24,25]. In particular, we tested several annealing conditions for $y = 0.4$, and the condition described in the "Methods" section was found to be the best. As shown in Fig. 3d, the lattice constant decreases with increasing *y*, which is a trend similar to other In-doped M–Te systems[8,12]. The actual element concentrations of the samples were examined by energy-dispersive X-ray spectroscopy (EDX), and the results are shown in Fig. S1 ("Supplementary information"). Basically, the actual compositions were close to the nominal values.

In Fig. 4, the temperature dependence of electrical resistivity of $AgSnBiTe_3$ ($x = 0.33$, $y = 0$) is displayed. Resistivity slightly decreases with decreasing temperature, and an increase in resistivity was observed at low temperatures. The result is consistent with the band calculations, based on SnTe lattice, in Fig. 2, and hence, the parent phase $AgSnBiTe_3$ would possess a narrow band gap. Since the calculated gap energy (Fig. 2e) indicates that a band inversion is expected for a metal telluride with $a = 6.2$ Å, $AgSnBiTe_3$ with $a = 6.20217(9)$ Å is expected to have topologically preserved electronic states near the Fermi energy (E_F). Thus, the In-substitution effects on physical properties of $AgSnBiTe_3$ are of interest because of the analogy to (Sn, In)Te, in which topological

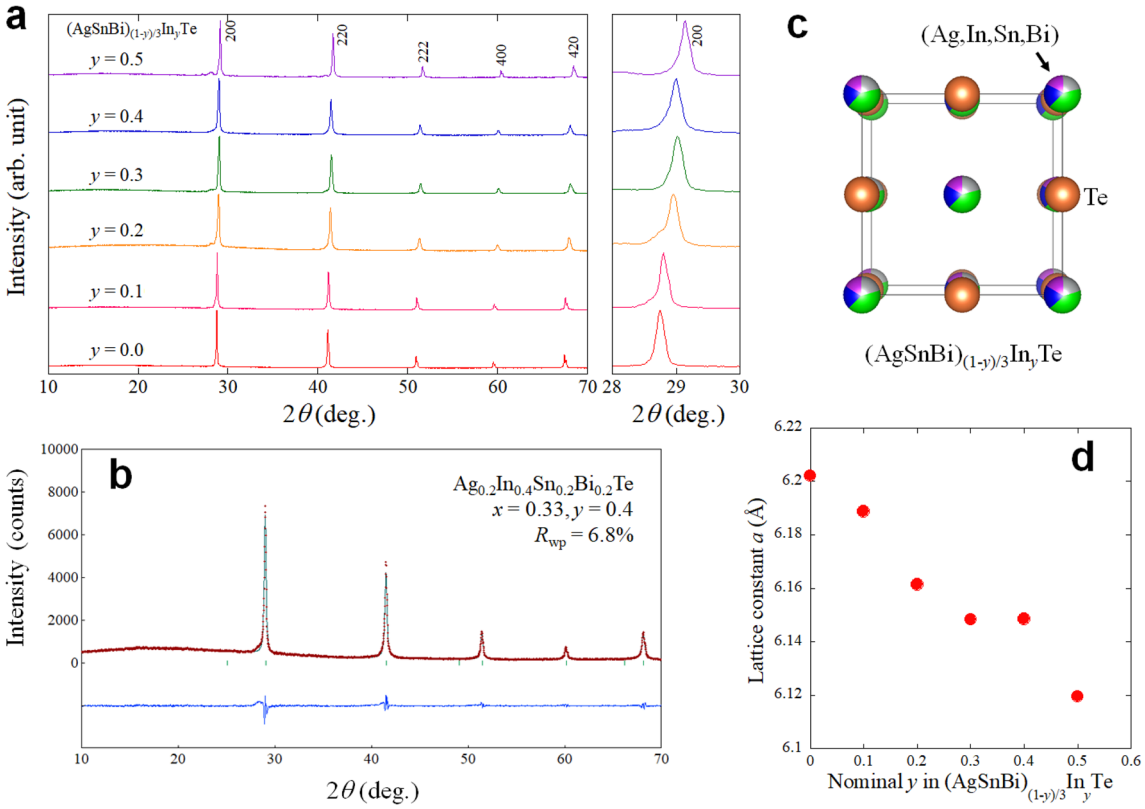

Figure 3. Crystal-structure evaluation of $(AgSnBi)_{(1-y)/3}In_yTe$. (**a**) XRD patterns of $(AgSnBi)_{(1-y)/3}In_yTe$. (**b**) Rietveld refinement result for $y = 0.4$. (**c**) Schematic image of the crystal structure. (**d**) y dependence of the lattice constant.

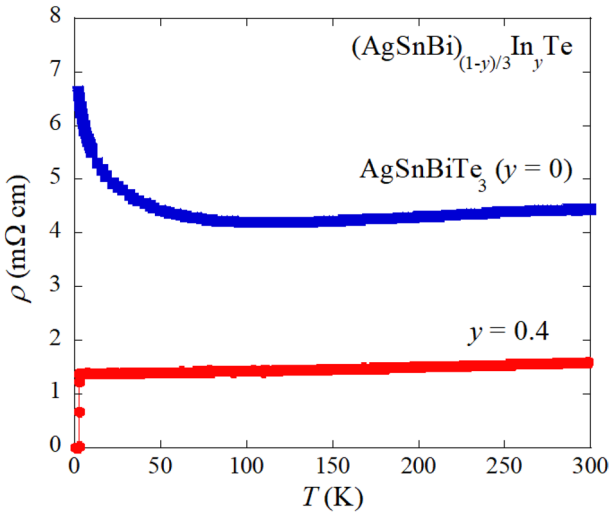

Figure 4. Temperature dependence of electrical resistivity for $y = 0$ ($AgSnBiTe_3$) and $y = 0.4$. In-doped ($y = 0.4$) sample shows a superconducting transition at $T = 2.4$ K.

superconductivity is expected to emerge. As expected, In-doped $AgSnBiTe_3$ shows superconductivity as displayed in Fig. 4. The resistivity data for $y = 0.4$ shows a metallic behavior and zero resistivity was observed at $T_c^{zero} = 2.4$ K. For the other samples with different In concentration, the temperature dependence of resistivity are shown in Fig. S2 ("Supplementary information"). The sample with $y = 0.1$ shows almost no temperature dependence in resistivity, but other samples ($y = 0.2$–0.5) show metallic conductivity.

To investigate upper critical field (B_{c2}), temperature dependences of resistivity were measured under various magnetic fields up to 1.5 T as plotted in Fig. 5a. For the estimation of B_{c2}, the transition temperature was

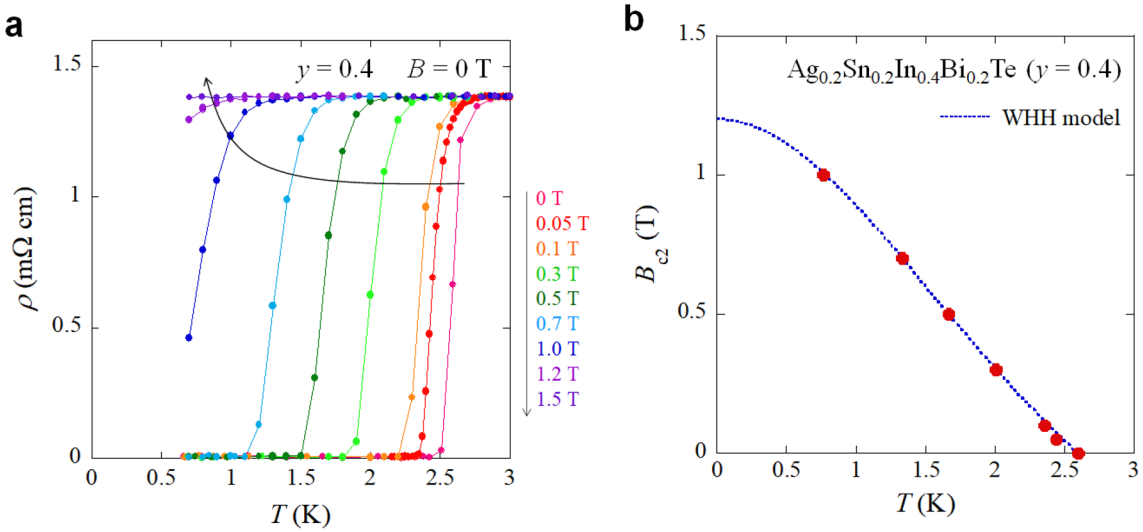

Figure 5. Estimation of upper critical field B_{c2} for $y = 0.4$. (**a**) Temperature dependences of resistivity under magnetic fields up to 1.5 T. With increasing field, the T_c systematically decreases. (**b**) Temperature dependence of B_{c2}. For the plot of B_{c2}, middle-point temperatures, where resistivity became 50% of normal-state resistivity at 3 K, were estimated in (**a**). The dotted line shows WHH fitting.

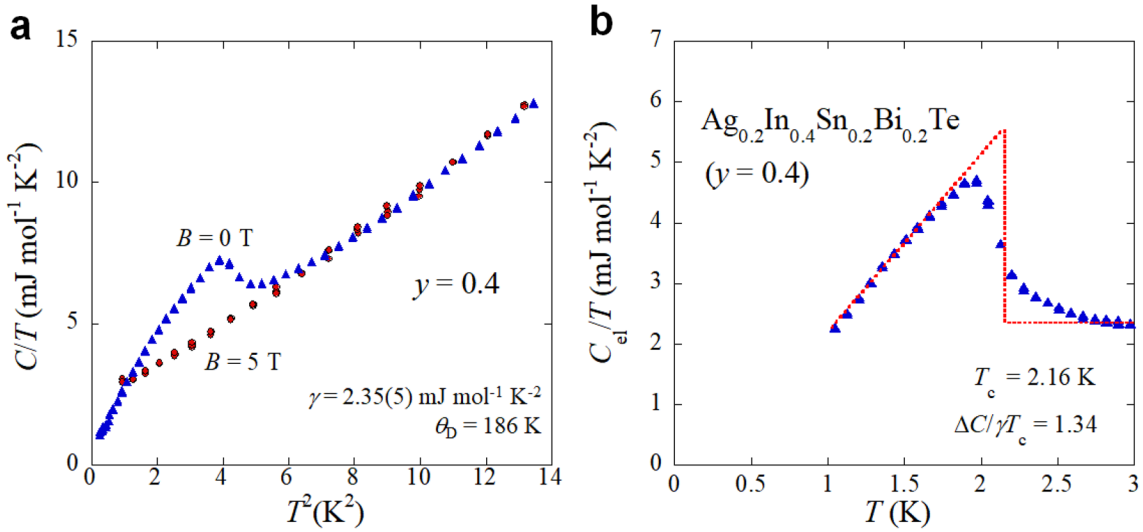

Figure 6. Specific heat data for $y = 0.4$. (**a**) Specific heat (C/T) data under magnetic fields (B) of 0 and 5 T plotted as a function of T^2. By fitting the data under $B = 5$ T, electronic specific heat parameter (γ) and Debye temperature (θ_D) were estimated. (**b**) Temperature dependence of the electronic contribution (C_{el}/T) under $B = 0$ T. The electronic contribution was calculated by subtracting the lattice contribution. T_c and the superconducting jump at T_c (ΔC) were estimated by considering the entropy balance, as guided by the red dashed lines. $\Delta C/\gamma T_c = 1.34$, which is close to BCS value of 1.43.

determined as a temperature where resistivity drops to 50% of the normal-state resistivity. Using the WHH model (Werthamer–Helfand–Hohenberg model)[26], which is applicable for a dirty-limit type-II superconductor, the $B_{c2}(0)$ was estimated as 1.2 T, as shown in Fig. 5b.

Figure 6 shows the analysis results of specific heat measurements. In Fig. 6a, specific heat data under 0 and 5 T in a form of C/T are plotted as a function of T^2. From the data under 5 T, the electronic specific heat parameter (γ) and the Debye temperature (θ_D) were estimated as 2.35(5) mJ mol^{-1} K^{-2} and 186 K, respectively. The low-temperature specific-heat formula with anharmonic term was used for the analysis: $C = \gamma T + \beta T^3 + \delta T^5$, where βT^3 is the lattice contribution to the specific heat, and the δT^5 term accounts for anharmonicity of the lattice. The θ_D was calculated from $\beta = (12/5)\pi^4(2N)k_B\theta_D^{-3}$, where N and k_B are the Avogadro constant and Boltzmann constant, respectively. To characterize the superconducting properties, the electronic contribution (C_{el}) under 0 T, which was calculated by subtracting lattice contributions from the specific heat data under 0 T, is plotted in the form of C_{el}/T as a function of temperature in Fig. 6b. The clear jump of C_{el}/T and decrease in C_{el}/T at low

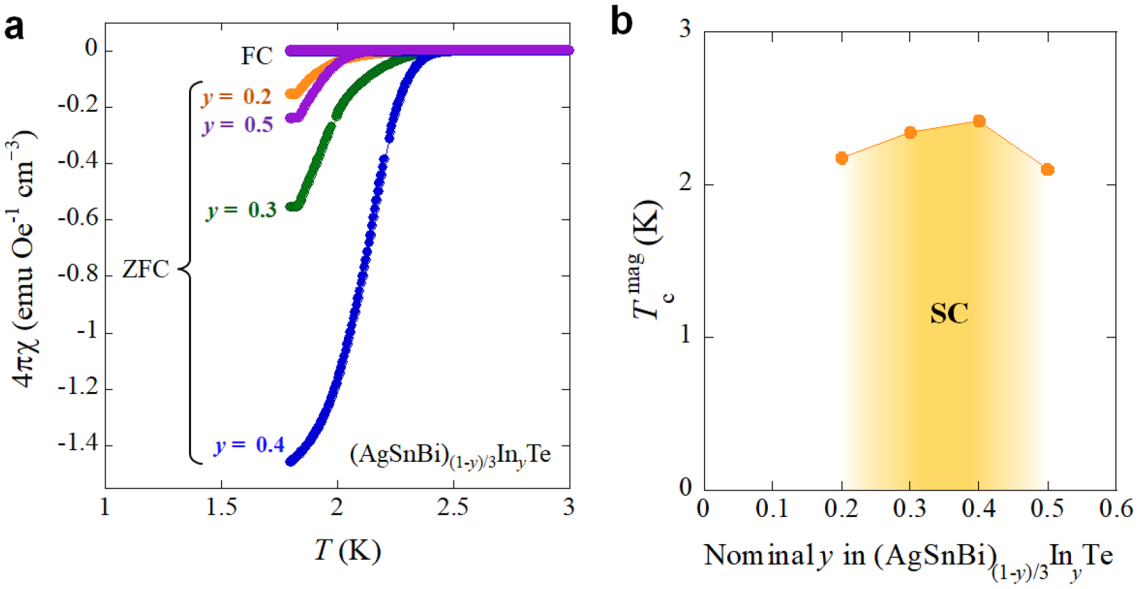

Figure 7. Magnetic susceptibility and superconducting transition temperature for $(AgSnBi)_{(1-y)/3}In_yTe$. (**a**) Temperature dependences of magnetic susceptibility ($4\pi\chi$) for $y = 0.2$, 0.3, 0.4, 0.5. (**b**) In concentration (y) dependence of T_c estimated from 1% shielding volume fraction (T_c^{mag}).

temperatures suggest the emergence of bulk superconductivity. The superconducting jump in C_{el} (ΔC_{el}) estimated with $T_c = 2.16$ K is $1.34\gamma T_c$, which is comparable to the value expected from a full-gap superconductivity based on the BCS model ($\Delta C_{el} = 1.43\gamma T_c$)[27]. Those values obtained from specific heat are similar to those obtained for In-doped SnTe and Ag-doped SnTe superconductors with 20% In (or Ag) doping[8,28].

To investigate the In-doping dependence of superconducting states, temperature dependences of magnetic susceptibility ($4\pi\chi$) was measured for $(AgSnBi)_{(1-y)/3}In_yTe$. For, $y = 0$ and 0.1, no superconducting transition was observed at temperatures above 1.8 K. Superconducting diamagnetic signals were observed for $y = 0.2$–0.5, as displayed in Fig. 7a. Particularly, samples with $y = 0.3$ and 0.4 showed a large shielding fraction. Note that the data has not been corrected by demagnetisation effect. The observation of the largest shielding volume fraction is consistent with the bulk superconductivity confirmed in specific heat measurements. As shown in Fig. 7b, T_c estimated from magnetic susceptibility (T_c^{mag}) becomes the highest at $y = 0.4$ and decreases with further In doping ($y = 0.5$).

The estimated T_c for $y = 0.4$ is lower than that for (Sn, In)Te ($T_c \sim 4.5$ K)[16]. The difference may be caused by three possible reasons: (1) carrier concentration, (2) the effect of disorder, and (3) lattice constant. On (1) carrier concentration, we performed measurements of Seebeck coefficient (at room temperature) and Hall coefficient (at 5 K for $y = 0.4$). Figure 8 shows the y dependence of Seebeck coefficient (S). For $y = 0$, a large positive value of S was observed. This is consistent with the band calculation, indicating that the parent phase of $y = 0$ is a semiconductor. With increasing y, S becomes negative, and the absolute value for $y > 0.1$ becomes less than 10 μV K^{-1}, which is a typical value of metals. In Fig. S3 ("Supplementary information"), the magnetic field dependence of Hall resistance at 5 K is plotted. By linear fitting of the data and assuming a single-band model, carrier concentration was calculated as 7.4×10^{21} cm^{-3}. These results on the evolution of carrier concentration by In substitution in $(AgSnBi)_{(1-y)/3}In_yTe$ would suggest that electrons are doped by In^{3+} substitution, and the doping situation in the present system is clearly different from that observed in (Sn, In)Te[16]. Therefore, to investigate the relationship between superconducting properties and carrier concentration in $(AgSnBi)_{(1-y)/3}In_yTe$, further investigation with various probes is needed. On the effect of (2) disorder, it is a fact that high configurational entropy of mixing is present at the M site as described in the following discussion. However, comparison of T_c between $y = 0.4$ (M = Ag, In, Sn, Bi) and other MTe superconductors, for example, M = In ($T_c \sim 3$ K)[9,12] and $M = Sn_{0.8}Ag_{0.2}$ ($T_c = 2.3$ K)[11], suggests that the higher disorder in $y = 0.4$ (M = Ag, In, Sn, Bi) is not highly affecting T_c. On the effect of (3) lattice constant, the electronic structure of SnTe-based materials is modified by lattice constant as shown above. In addition, in Ref.[25], we showed that T_c of MTe shows a positive relation to lattice constant. Therefore, the T_c obtained for $y = 0.4$ would be reasonable to the trend of T_c-lattice constant for MTe. According to those facts, we consider that the difference in T_c between $y = 0.4$ and (Sn, In)Te is caused by the difference in the electronic states (carrier concentration and/or lattice constant).

Solubility limit and phase stabilisation by configurational entropy of mixing. The doping phase diagram for superconductivity of $(AgSnBi)_{(1-y)/3}In_yTe$ is compared with that for the (Sn, In)Te and (Pb, In)Te systems in the following discussion. Having looked at the phase diagrams of (Sn, In)Te and (Pb, In)Te[8,12], superconductivity is observed in a wide range of In concentration. As shown in Fig. 7b, however, the superconducting properties (T_c and shielding volume fraction) becomes the highest for $y = 0.4$, and superconductivity seems to be suppressed for further In doping. Therefore, the trend of In-doping effect on superconductivity in the $AgSnBiTe_3$

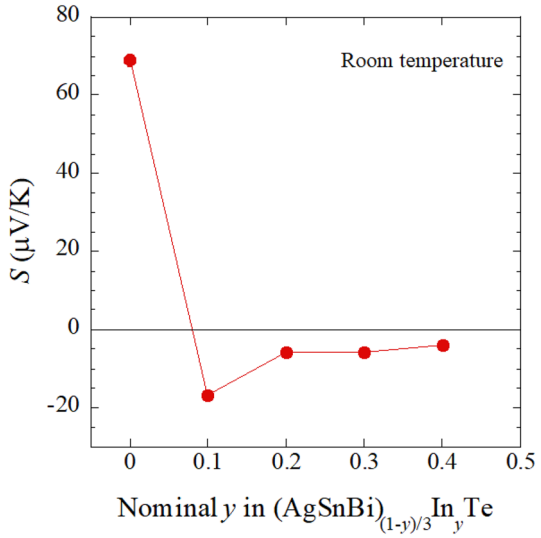

Figure 8. Effect of In doping on Seebeck coefficient (S) for $(AgSnBi)_{(1-y)/3}In_yTe$. In concentration (y) dependence of S at room temperature is shown.

system is different from that in the SnTe and PbTe systems. We consider that the suppression of superconductivity is caused by the solution limit of In rather than the changes in electronic states.

We tried to synthesise samples with $y > 0.5$, but a high-purity sample was not obtained. In addition, the Bi amount for $y = 0.5$ deviates from the nominal value with a large error, which means that the sample with $y = 0.5$ also contains inhomogeneity larger than those in $y < 0.5$. Seeing lattice constants for In-doped samples, we find that the lattice constant is smaller than the end member of InTe with $a \sim 6.175$ Å[8]. Therefore, we consider that the suppression of superconductivity observed for $y = 0.5$ is due to the increase in inhomogeneity in the sample, and the solution limit of In for $AgSnBiTe_3$ is around $y = 0.4$ under pressures up to 2 GPa. As a fact, $y = 0.4$ samples show degradation of superconducting properties by passing time. Thus, in this study, investigations of superconducting properties of $y = 0.4$ have been performed in 24 h after the high-pressure synthesis. Because the (Ag,In,Sn,Bi)Te system is a kind of disordered system with high configurational entropy of mixing (ΔS_{mix}), we briefly discuss the possible explanation of the solution limit of In in (Ag, In, Sn, Bi)Te. As established in a field of high-entropy alloys, the phase of multiple-element system can be stabilized owing to high ΔS_{mix}[29,30], which decreases Gibbs free energy, $\Delta G = \Delta H - T\Delta S$, at high temperatures, where H is enthalpy. ΔS_{mix} values for $Sn_{1-2x}(AgBi)_xTe$ and $(AgSnBi)_{(1-y)/3}In_yTe$ were calculated using $\Delta S_{mix} = -R\Sigma^i c_i \ln c_i$, where c_i and R are the atomic fraction of component i and the gas constant, respectively. As shown in Fig. 9a, for $Sn_{1-2x}(AgBi)_xTe$, ΔS_{mix} is relatively high with a wide range of x, which would be the reason why the phases could be obtained with a wide range of x without the use of high-pressure synthesis. For In doping, we selected $AgSnBiTe_3$ ($x = 0.33$) as a parent phase in this study. For $(AgSnBi)_{(1-y)/3}In_yTe$, ΔS_{mix} becomes the highest at $y = 0.3$, and it decreases with further In substitution, as shown in Fig. 9b. Therefore, the possible explanation of the solution limit of In for $AgSnBiTe_3$ is as follows. Due to the small lattice constant of ~ 6.2 Å for $AgSnBiTe_3$, In substitution was challenging, but the phase was stabilized up to $y = 0.4$ by the use of high pressure and high ΔS_{mix}. If we could get a phase with a higher In concentration, the superconducting phase diagram would be expanded from that shown in Fig. 7b.

Summary

We have synthesised polycrystalline samples of $Sn_{1-2x}(AgBi)_xTe$ and $(AgSnBi)_{(1-y)/3}In_yTe$ to explore a new candidate phase of topological superconductor. For $Sn_{1-2x}(AgBi)_xTe$, single-phase samples were obtained with a wide range of x. According to band calculations, we confirmed that the $Sn_{1-2x}(AgBi)_xTe$ system is basically possessing band inversion and topologically preserved electronic states. To investigate the effects of In substitution, we selected $x = 0.33$ ($AgSnBiTe_3$) as a parent phase. For $(AgSnBi)_{(1-y)/3}In_yTe$, In-doped samples were obtained for $y = 0$–0.5 by high-pressure synthesis, and superconductivity was observed for $y = 0.2$–0.5. For $y = 0.4$, specific heat investigation confirmed the emergence of bulk superconductivity. Although the current study is the material exploration with polycrystalline samples, we expect that the single crystals of (Ag,In,Sn,Bi)Te are grown in the next step, and characteristics including surface states, which are expected for a topological superconductor, are experimentally examined by surface-sensitive probes like angle-resolved photoemission spectroscopy.

Methods

Polycrystalline samples of $Sn_{1-2x}(AgBi)_xTe$ ($x = 0.00$, 0.05, 0.10, 0.15, 0.20, 0.25, 0.30, 0.33, 0.35, 0.40, 0.45) and $(AgSnBi)_{(1-y)/3}In_yTe$ ($y = 0.0$, 0.1, 0.2, 0.3, 0.4, 0.5) were prepared by a melting method in an evacuated quartz tube. Powders or grains of Ag (99.9% up), Sn (99.99%), Bi (99.999%), In (99.99%), and Te (99.999%) were mixed and melted in an evacuated quartz tube at 900 °C for 10 h, followed by furnace cooling to room temperature. For $(AgSnBi)_{(1-y)/3}In_yTe$, the obtained samples were powdered and annealed in a high-pressure-synthesis instrument

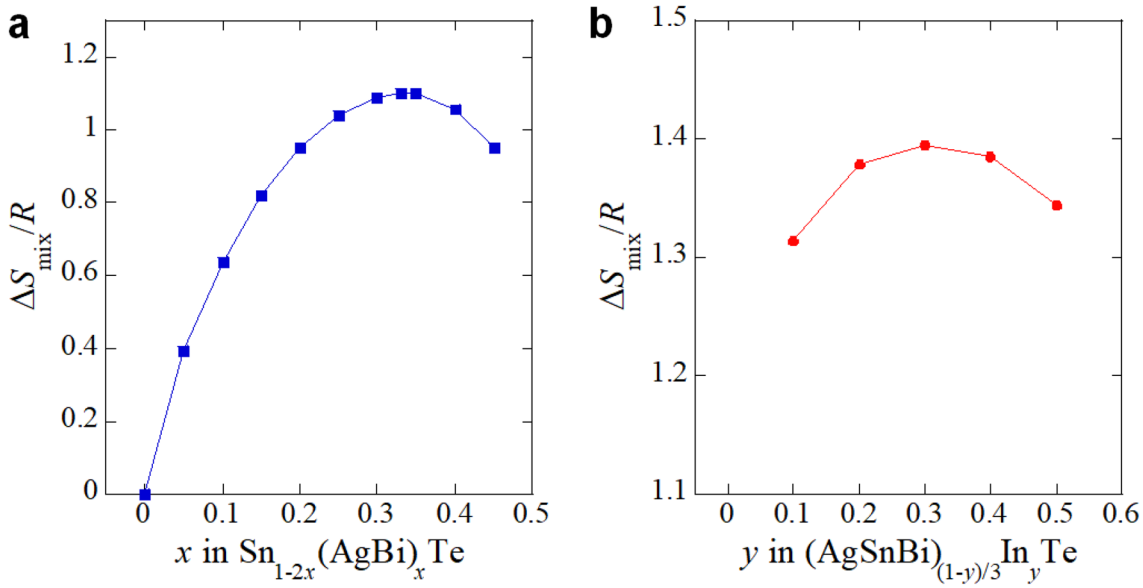

Figure 9. Configurational entropy of mixing (ΔS_{mix}). (**a**) x dependence of ΔS_{mix} for $Sn_{1-2x}(AgBi)_xTe$. (**b**) y dependence of ΔS_{mix} for $(AgSnBi)_{(1-y)/3}In_yTe$.

under 2 GPa at 500 °C for 30 min. A cubic-anvil-type 180-ton press was used, and the sample sealed in a BN crucible was heated by carbon heater.

The phase purity and the crystal structure of $Sn_{1-2x}(AgBi)_xTe$ and $(AgSnBi)_{(1-y)/3}In_yTe$ were examined by laboratory X-ray diffraction (XRD) by the θ–2θ method with a Cu–K_α radiation on a MiniFlex600 (RIGAKU) diffractometer equipped with a high-resolution detector D/tex Ultra. The schematic images of crystal structures were drawn by VESTA[31] using a structural data refined by Rietveld refinement using RIETAN-FP[32]. The actual compositions of the examined samples were analysed using an energy dispersive X-ray spectroscopy (EDX) on TM-3030 (Hitachi).

The temperature dependence of magnetic susceptibility was measured using a superconducting quantum interference devise (SQUID) on MPMS-3 (Quantum Design) after zero-field cooling (ZFC) with an applied field of 10 Oe. The temperature dependence of electrical resistivity was measured by a four-probe method with an applied DC current of 1 mA on PPMS (Quantum Design) under magnetic fields. We used Ag paste and Au wires (25 μm in diameter) for the four-probe setup. The temperature dependence of specific heat was measured under 0 and 5 T by a relaxation method on PPMS. The resistivity and specific heat measurements were performed using a ^{3}He probe system (Quantum Design). Hall coefficient was measured by four-probe setup on PPMS at low temperatures. Hall coefficient was estimated from the slope in the magnetic field dependence of Hall voltage. Seebeck coefficient at room temperature was measured under steady-state, where the thermo-electromotiveforce (ΔV) and the temperature difference (ΔT) were simultaneously measured, and the S was determined from the slope of $\Delta V/\Delta T$.

First principles band calculations were performed using WIEN2k package[33]. The electronic density of PbTe and SnTe was self-consistently calculated within the modified Becke–Johnson potential[34] using a $12 \times 12 \times 12$ k-mesh and $RK_{max} = 9$ with the spin–orbit coupling included.

Received: 16 September 2021; Accepted: 8 November 2021
Published online: 24 November 2021

References

1. Tanaka, Y. *et al.* Experimental realization of a topological crystalline insulator in SnTe. *Nat. Phys.* **8**, 800 (2012).
2. Hsieh, T. H. *et al.* Topological crystalline insulators in the SnTe material class. *Nat. Commun.* **3**, 982 (2012).
3. Ando, Y. Topological insulator materials. *J. Phys. Soc. Jpn.* **82**, 102001 (2013).
4. Sasaki, S. *et al.* Odd-parity pairing and topological superconductivity in a strongly spin–orbit coupled semiconductor. *Phys. Rev. Lett.* **109**, 217004 (2012).
5. Zhong, Y. *et al.* Optimized strategies for advancing n-type PbTe thermoelectrics: A review. *ACS Appl. Mater. Interfaces* **12**, 49323 (2020).
6. Zhang, Q. *et al.* High thermoelectric performance by resonant dopant indium in nanostructured SnTe. *Proc. Natl. Acad. Sci.* **110**, 13261 (2013).
7. Chen, Y. *et al.* SnTe–$AgSbTe_2$ thermoelectric alloys. *Adv. Energy Mater.* **2**, 58 (2012).
8. Kobayashi, K., Ai, Y., Jeschke, H. O. & Akimitsu, J. Enhanced superconducting transition temperatures in the rocksalt-type superconductors $In_{1-x}Sn_xTe$ ($x \leq 0.5$). *Phys. Rev. B* **97**, 104511 (2018).
9. Kriener, M. *et al.* Tailoring band structure and band filling in a simple cubic (IV, III)-VI superconductor. *Phys. Rev. Mater.* **2**, 044802 (2018).
10. Erickson, A. S. *et al.* Enhanced superconducting pairing interaction in indium-doped tin telluride. *Phys. Rev. B* **79**, 024520 (2009).

11. Mizuguchi, Y. & Miura, O. High-pressure synthesis and superconductivity of Ag-doped topological crystalline insulator SnTe ($Sn_{1-x}Ag_xTe$ with x = 0–0.5). *J. Phys. Soc. Jpn.* **85**, 053702 (2016).
12. Katsuno, M. et al. High-Pressure Synthesis and Superconducting Properties of NaCl-Type $In_{1-x}Pb_xTe$ (x = 0–0.8). Condens. Matter 5, 14 (2020).
13. Balakrishnan, G., Bawden, L., Cavendish, S. & Lees, M. R. Superconducting properties of the In-substituted topological crystalline insulator SnTe. *Phys. Rev. B* **87**, 140507 (2013).
14. Novak, M. *et al.* Unusual nature of fully gapped superconductivity in In-doped SnTe. *Phys. Rev. B* **88**, 140502 (2013).
15. Zhong, R. D. *et al.* Optimizing the superconducting transition temperature and upper critical field of $Sn_{1-x}In_xTe$. *Phys. Rev. B* **88**, 020505 (2013).
16. Haldolaarachchige, N. *et al.* Anomalous composition dependence of the superconductivity in In-doped SnTe. *Phys. Rev. B* **93**, 024520 (2016).
17. Ando, Y. & Fu, L. Topological crystalline insulators and topological superconductors: from concepts to materials. *Annu. Rev. Condens. Matter Phys.* **6**, 361 (2015).
18. Yan, C. *et al.* Experimental observation of Dirac-like surface states and topological phase transition in $Pb_{1-x}Sn_xTe(111)$ films. *Phys. Rev. Lett.* **112**, 186801 (2014).
19. Zhang, C. L. *et al.* Highly tunable topological system based on PbTe–SnTe binary alloy. *Phys. Rev. Mater.* **4**, 091201 (2020).
20. Du, G. *et al.* Fully gapped superconductivity in In-doped topological crystalline insulator $Pb_{0.5}Sn_{0.5}Te$. *Phys. Rev. B* **92**, 020512 (2015).
21. Tan, G. *et al.* SnTe–$AgBiTe_2$ as an efficient thermoelectric material with low thermal conductivity. *J. Mater. Chem. A* **2**, 20849 (2014).
22. Mashadieva, L. F. *et al.* The Ag_2Te–SnTe–Bi_2Te_3 system and thermodynamic properties of the $(2SnTe)_{1-x}(AgBiTe_2)_x$ solid solutions series. *J. Alloy Compd.* **219**, 310 (1995).
23. Springholz, G. Molecular beam epitaxy of IV-VI semiconductors: multilayers, quantum dots and device applications. in *Molecular Beam Epitaxy: From Research to Mass Production* (ed. Henini, M.) (Elsevier, 2013).
24. Mizuguchi, Y. Superconductivity in high-entropy-alloy telluride $AgInSnPbBiTe_5$. *J. Phys. Soc. Jpn.* **88**, 124708 (2019).
25. Kasem, M. R. *et al.* Superconducting properties of high-entropy-alloy tellurides M–Te (M: Ag, In, Cd, Sn, Sb, Pb, Bi) with a NaCl-type structure. *Appl. Phys. Express* **13**, 033001 (2020).
26. Werthamer, N. R., Helfand, E. & Hohenberg, P. C. Temperature and purity dependence of the superconducting critical field, Hc_2. III. Electron spin and spin–orbit effects. *Phys Rev.* **147**, 295 (1966).
27. Bardeen, J., Cooper, L. N. & Schrieffer, J. R. Microscopic theory of superconductivity. *Phys. Rev.* **106**, 162 (1957).
28. Mizuguchi, Y. *et al.* Specific heat and electrical transport properties of $Sn_{0.8}Ag_{0.2}Te$ superconductor. *J. Phys. Soc. Jpn.* **85**, 103701 (2016).
29. MacDonald, B. E. *et al.* Recent progress in high entropy alloy research. *JOM* **69**, 2024 (2017).
30. Ng, C. *et al.* Entropy-driven phase stability and slow diffusion kinetics in an $Al_{0.5}CoCrCuFeNi$ high entropy alloy. *Intermetallics* **31**, 165 (2012).
31. Momma, K. & Izumi, F. VESTA: A three-dimensional visualization system for electronic and structural analysis. *J. Appl. Crystallogr.* **41**, 653–658 (2008).
32. Izumi, F. & Momma, K. Three-dimensional visualization in powder diffraction. *Solid State Phenom.* **130**, 15–20 (2007).
33. Blaha, P. *et al.* WIEN2k: An APW+lo program for calculating the properties of solids. *J. Chem. Phys.* **152**, 074101 (2020).
34. Tran, F. & Blaha, P. Accurate band gaps of semiconductors and insulators with a semilocal exchange-correlation potential. *Phys. Rev. Lett.* **102**, 226401 (2009).

Acknowledgements

The authors thank O. Miura for experimental supports. This work was partly supported by JSPS KAKENHI (Grant nos. 18KK0076, 21H00151, and 21K18834) and Advanced Research Program under the Human Resources Funds of Tokyo (Grant number: H31-1).

Author contributions

Y.M. and Y.G. led the project. T.M. and Y.M. synthesised the samples. T.M. and Y.M. characterised the samples using XRD and EDX. T.M. performed the magnetization measurements. T.M., K.H., A.Y., R.K., R.H., T.D.M., Y.A., and Y.M. performed electrical resistivity and Hall measurements. T.M., M.R.K., A.Y., R.H., T.D.M., Y.A., and Y.M. performed specific heat measurements. M.R.K., T.K., and Y.M. performed Seebeck coefficient measurements. Theoretical calculations were carried out by H.U. This work was supervised in whole by Y.M., A.Y., and Y.G. The manuscript was written by H.U. and Y.M. with input from all coauthors.

Competing interests

The authors declare no competing interests.

Additional information

Supplementary Information The online version contains supplementary material available at https://doi.org/10.1038/s41598-021-02341-9.

Correspondence and requests for materials should be addressed to Y.M.

Reprints and permissions information is available at www.nature.com/reprints.

Publisher's note Springer Nature remains neutral with regard to jurisdictional claims in published maps and institutional affiliations.